Direct Measurement of Intermediate-Range Casimir-Polder Potentials

H. Bender, Ph. W. Courteille, C. Marzok, C. Zimmermann, and S. Slama

Physikalisches Institut, Eberhard Karls Universität Tübingen, Auf der Morgenstelle 14, D-72076 Tübingen, Germany

(Received 9 November 2009; published 22 February 2010)

We present the first direct measurements of Casimir-Polder forces between solid surfaces and atomic gases in the transition regime between the electrostatic short-distance and the retarded long-distance limit. The experimental method is based on ultracold ground-state Rb atoms that are reflected from evanescent wave barriers at the surface of a dielectric glass prism. Our novel approach does not require assumptions about the potential shape. The experimental data are compared to the theoretical predictions valid in the different regimes. They agree best with a full QED calculation.

DOI: 10.1103/PhysRevLett.104.083201 PACS numbers: 34.35.+a, 12.20.Fv, 51.70.+f

One of the results of most fundamental importance in quantum electrodynamics (QED) is the appearance of zero-point fluctuations of electromagnetic fields in vacuum, i.e., the vacuum energy. This energy leads only in very special cases to measurable effects. One example is the well-known Casimir and van der Waals forces [1,2]. In addition to their fundamental importance, a detailed understanding of these forces is crucial for testing new fundamental physics at short distances such as non-Newtonian gravitational forces [3,4]. Furthermore, they have important technological implications for the development of micromachines with nanoscale moving parts [5,6]. Today, Casimir forces between solids can be measured with high precision [7–9]. These measurements are all done with objects that are large compared to the relevant distances where Casimir forces become dominant. Therefore, the underlying theory contains the macroscopic properties of the objects, i.e., the dielectric functions. Moreover, also the geometry of the macroscopic bodies plays an important role due to the nonadditivity of Casimir forces. A much cleaner situation is given when the test object is microscopic. This is in good approximation true for a single atom. In this case the force by which the atom is attracted towards a surface is often referred to as the Casimir-Polder (CP) force. In the limits of short and long distances CP forces can be approximated by different power laws [1,10], in the transition regime the full QED integral must be solved.

In the last two decades many efforts have been made to measure CP forces including sophisticated approaches such as diffraction and interferometry of cold atom beams at thin transmission gratings [11,12] and quantum reflection of atoms from solid surfaces [13–16]. In these experiments CP forces were studied indirectly by fitting the coefficients of the theoretical surface potentials to the measured data. Direct methods that have been developed up to now can be divided into spectroscopic [17–20] and kinetic measurements [21,22]. In this article the transition regime is probed for the first time by a direct model-free measurement. This is done by reflecting ultracold atoms from evanescent wave barriers similar to previous work [21]. However, here we systematically vary the mirror potential and introduce a new data analysis which allows for the direct investigation of surface potentials at subwavelength distances from the surface. The new method makes use of a known repulsive potential $V_{\mathrm{EW}}(z)$ that is added to the unknown attractive surface potential $V_{\mathrm{SF}}(z)$ with the goal to generate a potential barrier. By varying the strength of $V_{\mathrm{EW}}(z)$, the height and the position of the barrier can be adjusted. The height is measured by reflecting cold atoms of a given energy. The position can be determined from the derivative of the barrier height with respect to the strength of $V_{\mathrm{EW}}(z)$. This last step is the key feature for reconstructing the unknown surface potential.

The experimental situation is shown in Fig. 1. An evanescent wave (EW) leaking out from the surface of a transparent substrate generates a repulsive dipole potential of the form

$$V_{\mathrm{EW}} = C_0 P \exp\left\{-2\frac{z}{z_0}\right\}, \tag{1}$$

with a constant C_0, laser power P and the field decay length z_0 [23]. The total potential is now the sum of the (attractive) unknown surface potential V_{SF} and the EW Potential

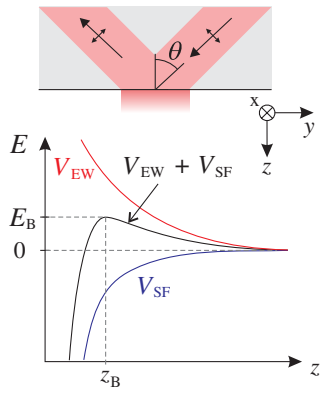

FIG. 1 (color online). Experimental situation. A repulsive evanescent wave potential V_{EW} and an attractive surface potential V_{SF} sum up to build a barrier at a distance z_B from the surface with height E_B.

$$V_{\mathrm{tot}} = V_{\mathrm{SF}} + V_{\mathrm{EW}}. \quad (2)$$

If the repulsive potential is strong enough, a potential barrier is formed at a distance $z_B(P)$ from the surface. At the maximum $V'_{\mathrm{tot}} = 0$, which means that

$$V'_{\mathrm{SF}}(z = z_B) = 2C_0 \frac{P}{z_0} \exp\left\{-2\frac{z_B}{z_0}\right\}. \quad (3)$$

Furthermore, the height of the barrier is given by

$$E_B = V_{\mathrm{SF}}(z_B) + C_0 P \exp\left\{-2\frac{z_B}{z_0}\right\}. \quad (4)$$

Differentiating (4) with respect to P, taking the inner derivatives into account (note that $z_B(P)$ is a function of P) and substituting Eq. (3) delivers:

$$\frac{dE_B}{dP} = C_0 \exp\left\{-2\frac{z_B}{z_0}\right\}. \quad (5)$$

The crucial point here is that this derivative depends only on the evanescent wave potential and not on the surface potential. From this expression the position of the barrier can be calculated to be

$$z_B(P) = -\frac{z_0}{2} \ln\left(\frac{1}{C_0}\frac{dE_B}{dP}\right). \quad (6)$$

With the knowledge of the barrier height E_B and the barrier position z_B the unknown surface potential $V_{\mathrm{SF}}(z_B)$ can be determined by solving (4).

The experimental task is to measure the height of the potential barrier as a function of the laser power. For a given laser power this is done by classical reflection of an ultracold atom cloud with variable kinetic energy from the barrier. The experiment is carried out with a setup explained in detail in [24]. Here only a short summary is given. An ultracold atomic cloud is prepared in a Joffe-Pritchard type trap some hundred micrometers below the superpolished surface of a dielectric glass prism which is mounted upside down in a vacuum chamber. Almost pure condensates can be generated with some 10^5 atoms. For this experiment however, only very cold thermal clouds are prepared in order to avoid effects due to the interaction between the atoms at high density. The ultracold ^{87}Rb cloud is held in the magnetic trap at a fixed distance z_1 below the prism surface. Then a vertical laser beam (wavelength $\lambda = 830$ nm) that propagates perpendicularly through the prism from the top is switched on adiabatically in order to generate a dipole trap with radial and axial trapping frequencies of $\omega_{d,r} = 2\pi \times 50$ Hz and $\omega_{d,z} < 2\pi \times 0.1$ Hz. In this combined magnetic-dipole trap a cloud temperature of $T \sim 100$ nK is measured. Now the atoms are accelerated towards the surface by a sudden shift of the magnetic trapping minimum to a new variable position z_2. After a waiting time of a quarter of an oscillation period during which the atoms accelerate in the shifted trap, the magnetic field is quickly ramped to a constant gradient which compensates for the gravitational force. The atoms now move towards the surface with a nearly constant velocity v_0. It is determined by absorption imaging of the position of the cloud in the first few milliseconds of its motion. While the atoms move to the surface they are slightly accelerated due to residual curvature of the levitation potential. This effect is taken into account as a correction of the measured velocity. The velocity at the surface is then given by $v = \sqrt{v_0^2 + \omega_{\mathrm{lev}}^2 z_2^2}$ with $\omega_{\mathrm{lev}} = 2\pi \times 4$ Hz. During the reflection of the atoms the dipole trap guarantees radial confinement. The measured radial FWHM width of the atomic cloud is 40 μm such that the atoms are reflected only from the center of the evanescent wave. There, the potential barrier reaches its maximum due to the Gaussian intensity distribution of the EW laser spot. The EW laser is centered around $\lambda = 765$ nm with a spectral width of $\Delta\lambda = \pm 1$ nm. The vertical potential generated by the dipole trap is very weak and can be neglected. After contact with the surface the number of reflected atoms is determined by absorption imaging. The measurement is repeated for various trap displacements $\Delta z = z_2 - z_1$ which correspond to different velocities v. Typical results are shown in the inset of Fig. 2. The data points show a gradual decrease from the situation where all atoms are reflected ($R = 1$) to full transmission $R = 0$. The width of this decrease is mainly dominated by the Gaussian velocity distribution of the atoms corresponding to the temperature of the cloud. It is also slightly affected by the inhomogeneous barrier height due to the Gaussian transverse intensity profile of the EW laser beam. Nonclassical broadening effects like quantum reflection and tunneling may play a role for the higher laser powers used, where the surface potential is steepened by the evanescent wave [25]. However, its influence on the center of the decrease and by that on the measured barrier height is negligible. Thus the data points in Fig. 2 are fit with a model which implements only the two classical broadening mechanisms mentioned above. The result of the fits for various laser powers is plotted in the main part of Fig. 2 (open circles). For comparison, barrier heights are plotted as derived from the theoretical CP potentials valid in the different regimes:

$$V_{\mathrm{CP}} = \begin{cases} V_{\mathrm{vdW}} = -\frac{C_3}{z^3} & (z \gg l), \\ V_{\mathrm{ret}} = -\frac{C_4}{z^4} & (z \ll l), \end{cases} \quad (7)$$

with a typical distance l separating both regimes. For calculating the potential coefficients C_j the values for an ideally conducting surface C_j^{ic} are taken from [26] and corrected for the dielectric surface. In the case of the C_4 coefficient the correction is given by a factor $\Phi(n)$ with refractive index $n = 1.512$ [2]. In the case of the C_3 coefficient an often made approximation leads to a correction factor of $\frac{n-1}{n+1}$. Our corrected coefficients are $C_3 = 5.8 \times 10^{-49}$ J m^3 and $C_4 = 5.4 \times 10^{-56}$ J m^4. The transition length can be estimated from the intersection between

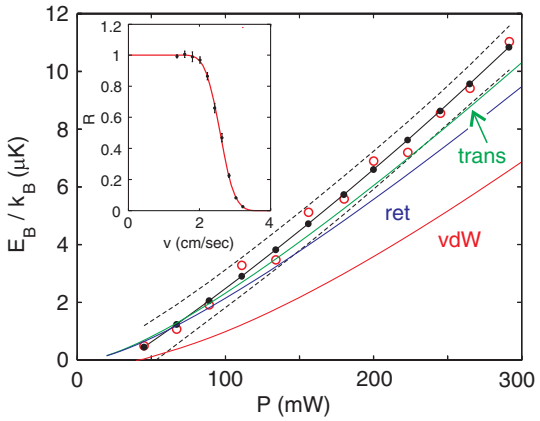

FIG. 2 (color online). Inset: Typical measurement of reflectivity R for a laser power of $P = 134$ mW. The fitted barrier height is $E_B = k_B \times (3.62 \pm 0.03)$ μK. Main figure: Dependence of the barrier height on the laser power. The open circles are data points obtained from curves similar to the ones shown in the inset. The solid line close to the data points is a constraint fit to the data as explained in the text with the dashed lines limiting the 95% confidence interval. The three curves (vdW, ret, trans) are theoretical expectations for the barrier height assuming a nonretarded van der Waals-like potential, a retarded potential and the full QED potential.

the retarded and the nonretarded curve to be $l \approx \frac{C_4}{C_3} = 92$ nm. In this range we calculate the Casimir-Polder potential correctly by solving the full QED formula (5.39) in [27]. For this purpose the magnetic permeability of glass is $\mu(\omega) \equiv \mu = 1$ and the atomic polarizability $\alpha(\omega)$ follows from [28]. The dielectric function $\epsilon(\omega)$ is determined from optical data which are available for glass in a wide range [29]. The barrier height which is derived from this correct CP potential fits best to the experimental data, although also here a deviation is observed. This deviation is particularly large for high laser powers, where the data exceed the theoretical values. A model-free comparison between experiment and theory is possible, if the surface potential is extracted from the measurement as explained above. The required derivative $\frac{dE_B}{dP} \approx \frac{E_B(n+1)-E_B(n)}{P(n+1)-P(n)}$ is taken from a smoothened curve that can be obtained by fitting the measured barrier heights. The fit function must be chosen very carefully in order to stay model-free. A polynomial fit function, e.g., would implicitly assume a surface potential of a certain shape. To maintain generality the values of the fit function at the measured laser powers are the parameters of the fit. Furthermore, the fit function fulfils the following three constraints: (1) the first derivative is positive at each point, (2) the second derivative is also positive at each point, and (3) the third derivative is negative at each point. The physical reason for (1) is that an increasing laser power leads to a growing barrier height. Constraint (2) is equivalent to the fact that for increasing laser power the barrier gets closer to the surface and constraint (3) means that the rate at which the barrier gets closer to the surface decreases. These assumptions are valid for any attractive surface potential whose attraction is growing with decreasing distance from the surface. This is the only assumption on the potential shape we make. The result of the fit is plotted as dots in Fig. 2. To guide the eye the fit points are linearly interpolated. From the fit points the surface potential is determined by Eqs. (4) and (6). The only parameters in this calculation are the ones describing the evanescent wave: the field decay length z_0 is calculated from a measured incidence angle of $\theta = 43.4° \pm 0.1°$, and a laser wavelength of $\lambda = 765$ nm to $z_0 = (430 \pm 10)$ nm. The proportionality factor C_0 is calculated from standard dipole trap theory [23] with a measured beam waist of $w_{0,x} = (170 \pm 5)$ μm and $w_{0,y} = (227 \pm 5)$ μm. The evanescent wave intensity is given (for p-polarized light) by $|\frac{E_{\mathrm{EW}}}{E_{\mathrm{in}}}|^2 = \frac{1}{n}\frac{4n^2\cos(\theta)^2}{[\cos(\theta)^2+n^2\{n^2\sin(\theta)^2-1\}]}$, with the refractive index n of the prism. With these parameters the proportionality constant is $C_0 = (1.38 \pm 0.05) \times 10^{-27}$ J/W [30].

Figure 3 shows the surface potential determined from the measured barrier height (dots). Statistical errors are due to the spread of the data points in Fig. 2 around the fit curve. For the vertical axis they are given by a shift of the fit curve to the 95% confidence interval boundaries. For the horizontal axis the evaluation of the statistical error depends on the error of the gradient of the fit curve. An estimation of this error can be given by calculating the mean gradient and assuming a maximum gradient by a linear interpolation between the lower left border of the confidence interval with the upper right border. For the minimum gradient the upper left border is connected with the lower right border. This gives an uncertainty in the gradient $\delta(\frac{dE_B}{dP})$. The uncertainty of the barrier position δz_B is then given by means of (6). Systematic errors are due to the uncertainty for z_0, C_0, P and v. Taking into account these uncertainties the measurements agree best with the full QED calculation. The retarded and the static potential can be excluded. Other experiments show that patch potentials from adsorbed Rubidium atoms can play a role in the surface potential [31]. Such potentials increase the attraction between surface and atom. An increase is also expected from charged particles at the surface and from photoinduced modifications of atom-surface interactions, as described in [32]. In contrast, our measurements show a slightly smaller attraction than theoretically expected. Therefore, additional attractive potentials seem to be negligible. For the patch potentials this might be due to a permanent exposure of the prism surface to the evanescent wave which can either lead to laser-induced desorption of atoms [33] or to an increased diffusion of atoms on the surface. Charged particles seem to exist only in small number on the surface, and laser-induced modifications of surface forces (e.g., by the EW) are calculated to be negligible due to the large detuning used in this setup.

In this article direct measurements of the Casimir-Polder force between ground-state Rb atoms and the surface of a dielectric glass prism at distances between 160 nm and

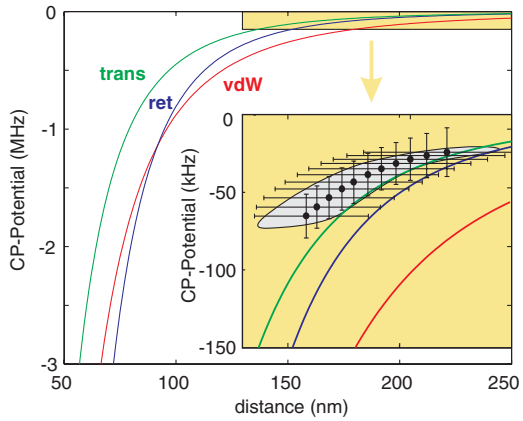

FIG. 3 (color online). Measured and theoretical Casimir-Polder potentials: in the large figure the theoretical surface potentials are plotted, i.e., the nonretarded van der Waals potential (vdW) and the retarded Casimir-Polder potential (ret). The full theoretical curve also valid in the transition regime (trans) approaches the retarded curve for large distances and the nonretarded curve for small distances. The inset magnifies the colored box, in which the measured data points are lying. Statistical and systematic errors are indicated by the error bars, and the grey shaded area, respectively.

230 nm are presented. A novel method has been introduced which is based on a test potential generated with an optical evanescent wave at the glass surface. The measurements do not coincide with the limiting formulas valid in the static and in the retarded regime. A better agreement is reached with the full QED calculation, although also here a deviation is observed. In addition to the mentioned measurement errors, this deviation might be caused by the imprecise knowledge of the dielectric function of the used borosilicate glass prism. For calculating the theoretical curve the well-known dielectric function of SiO_2 glass has been used. However, the optical properties of glasses vary depending on the exact type of glass [34]. It is therefore possible that the theoretical curve slightly deviates from the real situation in the experiment. Already a moderate increase in the experimental resolution will make it possible to discern between such theoretical and experimental errors.

We acknowledge financial support by the DFG within the EuroCors program of the ESF. We would like to thank Stefan Scheel and Andreas Günther for helpful discussions.

[1] H. B. G. Casimir and D. Polder, Phys. Rev. **73**, 360 (1948).
[2] I. Dzyaloshinskii, E. Lifshitz, and L. Pitaevskii, Adv. Phys. **10**, 165 (1961).
[3] R. Onofrio, New J. Phys. **8**, 237 (2006).
[4] R. S. Decca *et al.*, Phys. Rev. D **75**, 077101 (2007).
[5] E. Buks and M. L. Roukes, Phys. Rev. B **63**, 033402 (2001).
[6] F. W. DelRio *et al.*, Nature Mater. **4**, 629 (2005).
[7] F. Chen and U. Mohideen, J. Phys. A **39**, 6233 (2006).
[8] C. Hertlein, L. Helden, A. Gambassi, S. Dietrich, and C. Bechinger, Nature (London) **451**, 172 (2008).
[9] A. D. Corwin and M. P. deBoer, J. Microelectromech. Syst. **18**, 250 (2009).
[10] J. E. Lennard Jones, Trans. Faraday Soc. **28**, 333 (1932).
[11] R. E. Grisenti, W. Schöllkopf, J. P. Toennies, G. C. Hegerfeldt, and T. Köhler, Phys. Rev. Lett. **83**, 1755 (1999).
[12] J. D. Perreault and A. D. Cronin, Phys. Rev. Lett. **95**, 133201 (2005).
[13] F. Shimizu, Phys. Rev. Lett. **86**, 987 (2001).
[14] V. Druzhinina and M. DeKieviet, Phys. Rev. Lett. **91**, 193202 (2003).
[15] T. A. Pasquini, Y. Shin, C. Sanner, M. Saba, A. Schirotzek, D. E. Pritchard, and W. Ketterle, Phys. Rev. Lett. **93**, 223201 (2004).
[16] B. S. Zhao, S. A. Schulz, S. A. Meek, G. Meijer, and W. Schöllkopf, Phys. Rev. A **78**, 010902(R) (2008).
[17] V. Sandoghdar, C. I. Sukenik, E. A. Hinds, and S. Haroche, Phys. Rev. Lett. **68**, 3432 (1992).
[18] C. I. Sukenik, M. G. Boshier, D. Cho, V. Sandoghdar, and E. A. Hinds, Phys. Rev. Lett. **70**, 560 (1993).
[19] H. Failache, S. Saltiel, M. Fichet, D. Bloch, and M. Ducloy, Phys. Rev. Lett. **83**, 5467 (1999).
[20] M. Fichet *et al.*, Europhys. Lett. **77**, 54 001 (2007).
[21] A. Landragin *et al.*, Phys. Rev. Lett. **77**, 1464 (1996).
[22] J. M. Obrecht, R. J. Wild, M. Antezza, L. P. Pitaevskii, S. Stringari, and E. A. Cornell, Phys. Rev. Lett. **98**, 063201 (2007).
[23] R. Grimm, M. Weidemüller, and Y. B. Ovchinnikov, Adv. At. Mol. Opt. Phys. **42**, 95 (2000).
[24] H. Bender, P. Courteille, C. Zimmermann, and S. Slama, Appl. Phys. B **96**, 275 (2009).
[25] S. Kallush, B. Segev, and R. Côté, Eur. Phys. J. D **35**, 3 (2005).
[26] H. Friedrich, G. Jacoby, and C. G. Meister, Phys. Rev. A **65**, 032902 (2002).
[27] S. Scheel and S. Y. Buhmann, Acta Phys. Slov. **58**, 675 (2008).
[28] M. S. Safronova, C. J. Williams, and C. W. Clark, Phys. Rev. A **69**, 022509 (2004).
[29] E. D. Palik, *Handbook of Optical Constants of Solids* (Academic Press Inc., London, 1985).
[30] On the calculation of C_0: For the given incident linear polarization in the yz plane the EW is elliptically polarized. At the given incidence angle and the magnetic field directing into the positive x direction the light intensity can be decomposed into a 88% linearly and a 12% circularly σ^+ polarized fraction. The dipole potential is the given by formula (19) in [23], with $m_F = 2$.
[31] J. M. McGuirk, D. M. Harber, J. M. Obrecht, and E. A. Cornell, Phys. Rev. A **69**, 062905 (2004).
[32] J. D. Perreault, M. Bhattacharya, V. P. A. Lonij, and A. D. Cronin, Phys. Rev. A **77**, 043406 (2008).
[33] A. Hatakeyama, M. Wilde, and K. Fukatani, e-J. Surf. Sci. Nanotech. **4**, 63 (2006).
[34] A. M. Evimov and V. G. Pogareva, Chem. Geol. **229**, 198 (2006).